

# Nitrogen fixation in the North Atlantic supported by Gulf Stream eddy-borne diazotrophs

Received: 9 December 2023

Accepted: 18 September 2024

Published online: 11 October 2024

 Check for updates

Cora Hoerstmann<sup>1,2,3</sup>✉, Borja Aguiar-González<sup>4</sup>✉, Stéphanie Barrillon<sup>2</sup>, Cécile Carpaneto Bastos<sup>2,3</sup>, Olivier Grosso<sup>2</sup>, M. D. Pérez-Hernández<sup>5</sup>, Andrea M. Doglioli<sup>2</sup>, Anne A. Petrenko<sup>2</sup>, Lidia I. Carracedo<sup>6</sup> & Mar Benavides<sup>2,3,7</sup>✉

Mesoscale oceanic eddies contribute to the redistribution of resources needed for plankton to thrive. However, due to their fluid-trapping capacity, they can also isolate plankton communities, subjecting them to rapidly changing environmental conditions. Diazotrophs, which fix dinitrogen (N<sub>2</sub>), are key members of the plankton community, providing reactive nitrogen, particularly in large nutrient-depleted regions such as subtropical gyres. However, there is still limited knowledge about how mesoscale structures characterized by specific local environmental conditions can affect the distribution and metabolic response of diazotrophs when compared with the large-scale dynamics of an oceanic region. Here we investigated genetic diazotroph diversity and N<sub>2</sub> fixation rates in a transect across the Gulf Stream and two associated eddies, a region with intense mesoscale activity known for its important role in nutrient transport into the North Atlantic Gyre. We show that eddy edges are hotspots for diazotroph activity with potential community connectivity between eddies. Using a long-term mesoscale eddy database, we quantified N<sub>2</sub> fixation rates as up to 17 times higher within eddies than in ambient waters, overall providing ~21 μmol N m<sup>-2</sup> yr<sup>-1</sup> to the region. Our results indicate that mesoscale eddies are hotspots of reactive nitrogen production within the broader marine nitrogen cycle.

The Gulf Stream (GS) and associated mesoscale eddies enhance nutrient transport and biological productivity in the North Atlantic<sup>1</sup>, acting as ‘mini-engines of biogeochemical cycles’ in these otherwise low-productivity waters<sup>2</sup>. Within the planktonic community, dinitrogen (N<sub>2</sub>)-fixing cells (‘diazotrophs’) play a central role in marine productivity, as they provide a substantial amount (223 ± 30 Tg N yr<sup>-1</sup>) of reactive nitrogen globally<sup>3</sup>. Diazotrophs balance nitrogen budgets, particularly where the input of other nitrogen sources is limited, such as in the North Atlantic Gyre<sup>4</sup>. Although mesoscale eddies are recurrent features in the

North Atlantic<sup>5</sup>, the resolution of most in situ sampling is too coarse, limiting our understanding of how they affect diazotroph community structure and related N<sub>2</sub> fixation input.

The impact of mesoscale eddies on plankton communities is typically assessed by combining altimetry-derived currents and ocean colour observations<sup>6</sup>. However, remote sensing observations do not allow a study of the impacts of physical processes on functional changes within the planktonic community. For example, eddy rotation tends to isolate water masses in its core, which can result in either (1) trapped

A full list of affiliations appears at the end of the paper. ✉ e-mail: [cora.hoerstmann@awi.de](mailto:cora.hoerstmann@awi.de); [borja.aguiar@ulpgc.es](mailto:borja.aguiar@ulpgc.es); [mar.benavides@noc.ac.uk](mailto:mar.benavides@noc.ac.uk)

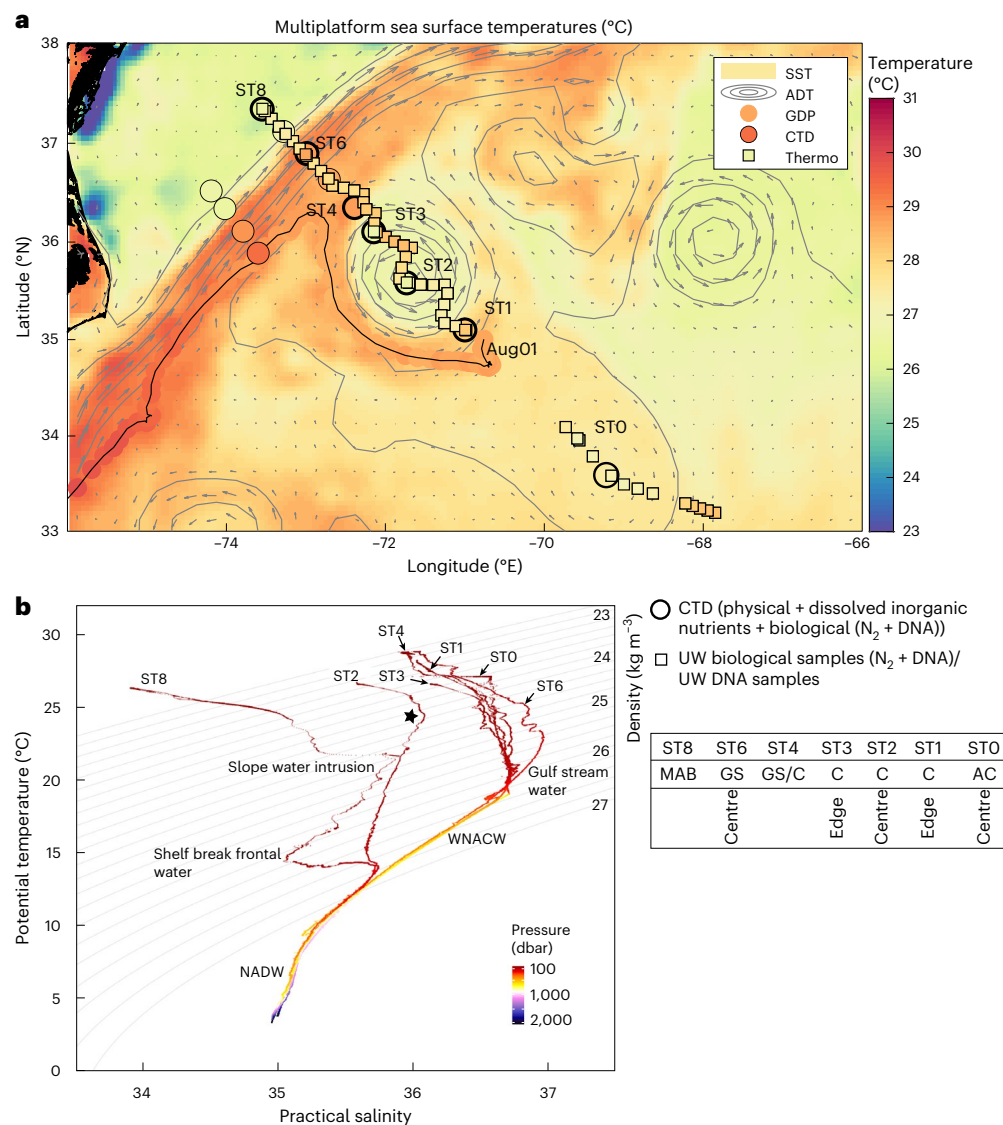


**Fig. 1** GS eddies with trapped shelf water and mixed water masses in the periphery. **a**, Multiplatform sea surface temperature measurements during the FIGURE-CARING cruise (RV AE2215), with data from satellite sea surface temperature (SST), conductivity–temperature–depth (CTD) stations and underway (UW) samples. Stations are classified into anticyclonic eddy (AC), cyclonic eddy (C), GS and MAB and separated into the centre or edge of the

structures. ADT, absolute dynamic topography. GDP, Global Drifter Program. **b**,  $\theta$ - $S$  diagram for ST0–ST8 colour-coded along pressure gradients. Water masses are indicated within the plot (NADW, North Atlantic Deep Water; WNACW, Western North Atlantic Central Water) and the black star indicates the entrained shelf water in the core of the cyclonic eddy.

species adapting their activity to the local environmental conditions or (2) other species with better adaptive capabilities becoming dominant, which then alters microbial diversity locally<sup>7</sup>. Similarly, eddies have been shown to modulate diazotroph abundance through isolation and changes in the tilting of the isopycnals that lead to changes in resource availability<sup>8</sup>, temperature<sup>9</sup>, passive accumulation of buoyant cells<sup>10,11</sup> and/or intensification or diminution of biological interactions such as grazing and viral lysis<sup>12–14</sup>. Anticyclonic eddies are considered hotspots for  $N_2$  fixation through their substantial depletion of other nitrogen sources<sup>10</sup>. In contrast, cyclonic eddies have been observed to feature fewer diazotrophs than the water masses of origin<sup>15</sup>. However, counter-intuitively, the opposite has also been observed, potentially associated with variable nutrient inputs over the eddy's life history<sup>10,16</sup>. Notably, diazotroph cell abundances do not necessarily equate to  $N_2$  fixing rates<sup>17</sup>. For example, not all diazotrophs fix  $N_2$  at the same efficiency, with a notable impact on the over- or underestimation of  $N_2$  fixation<sup>18</sup>. Therefore, combined diversity and  $N_2$  fixation measurements open a

window into the mechanisms shaping diazotroph diversity and quantitative activity changes across mesoscale structures.

In this Article we investigate diazotroph diversity and activity at submesoscale resolution across the GS and two counterrotating GS eddies (Fig. 1). Then, we measure the functional and phylogenetic responses of diazotrophs to the contrasting environmental conditions encountered in our field experiment. Finally, we quantify the recurrence of GS-associated mesoscale eddies to scale the influence of eddy-associated  $N_2$  fixation activity on nitrogen inputs in the western North Atlantic.

## Results and discussion

### GS eddies support $N_2$ fixation in the North Atlantic

In July–August 2022, we performed high-spatial-resolution transects (DNA samples every ~10 km,  $N_2$  fixation measurements every ~30 km) on two counterrotating GS eddies. The highest absolute  $N_2$  fixation rates (up to 52.73 nmol  $N_2$   $l^{-1}$   $d^{-1}$ ; ST8) occurred west of the GS in the Mid-Atlantic

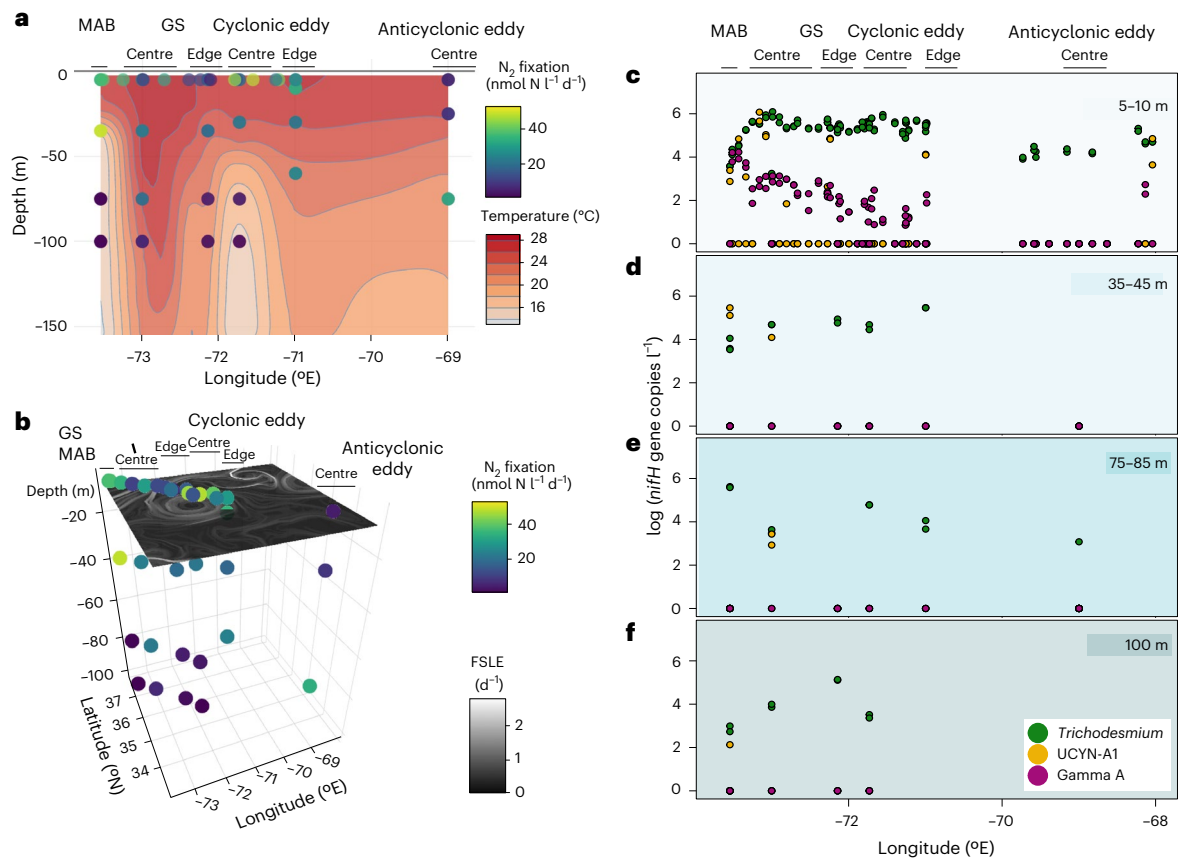


**Fig. 2 |  $N_2$  fixation and diazotroph abundance.** **a**,  $N_2$  fixation rates in nanomoles of N per litre per day against interpolated water temperature as derived using CTD measurements. **b**,  $N_2$  fixation rates in nanomoles of N per litre per day with the satellite product of finite-size Lyapunov exponent (FSLE) plotted at

the surface. **c–f**, Diazotroph abundance for different depth ranges (**c**, 5–10 m; **d**, 35–45 m; **e**, 75–85 m; **f**, 100 m) as measured by quantitative PCR (qPCR) targeting *Trichodesmium*, UCYN-A1 and Gamma A with cell counts normalized to a logarithmic scale.

Bight (MAB) at 35 m depth. However,  $N_2$  fixation remained notably high throughout the transect (Fig. 2a,b and Supplementary Table 1), with significantly higher rates than in previous studies in the North Atlantic Gyre (Welch two-sample *t*-test,  $P = 3.836 \times 10^{-6}$ ,  $n_1 = 22$ ,  $n_2 = 20$ ; Supplementary Data 1). Rates in these ranges have only been observed at these latitudes in the MAB (up to  $130 \text{ nmol N l}^{-1} \text{ d}^{-1}$ )<sup>19,20</sup>. While  $N_2$  fixation mostly decreased with depth, we found consistently high rates ( $>20 \text{ nmol N l}^{-1} \text{ d}^{-1}$ ) at depth in the eastern edge of the cyclonic eddy (ST1) and locally even increasing with depth at the centre of the anticyclonic eddy (ST0). These patterns of  $N_2$  fixation suggest that the vertical transport of diazotrophs may have promoted high  $N_2$  fixation at depth<sup>21</sup>.

The relatively high  $N_2$  fixation measurements during our survey can be linked to (1) trapping of shelf water enriched with diazotrophs, known for high  $N_2$  fixation activity<sup>19</sup> and accumulation in convergence zones<sup>12,22</sup>, and (2) upwelling and mixing providing excess phosphate and enhancing  $N_2$  fixation<sup>23,24</sup> (Supplementary Fig. 1). Higher water mass similarities between the MAB and the cyclonic eddy than to the GS or North Atlantic Gyre support the importance of the first mechanism (Fig. 1b). Trapping highly active diazotrophs in the core of the cyclonic eddy in combination with a positive  $P^*$  supported  $N_2$  fixation locally. Yet, no excess phosphate was observed at the edges of the cyclonic eddy with elevated  $N_2$  fixation across depth. Therefore, the transport of diazotrophs appears to be more important in driving  $N_2$  fixation in cyclonic eddies than the presence of other sources of nitrogen<sup>12,25</sup>. This shows the overall importance of trapping eddies in supporting  $N_2$  fixation in one of the world's most mesoscale-active regions, raising questions about their impact on other western boundary currents with similar observations<sup>26,27</sup>.

### Cyclonic eddy origin is linked to high $N_2$ fixation

To understand how the water mass and associated transported diazotroph communities within the core of the cyclonic eddy were shaped by its source water mass(es), we focused on the origin and maturity of the cyclonic eddy sampled across multiple stations and depths. We tracked its origin and identified its characteristics from the global Mesoscale Eddy Trajectory Atlas (META3.0exp NRT, hereafter NRT Eddy Atlas)<sup>28</sup> (Supplementary Video 1) and through a multiplatform approach (Fig. 1 and Supplementary Figs. 2–5). The trajectories of drifters and Argo floats indicated that the cyclonic eddy had a high trapping capacity (Supplementary Fig. 2) and was horizontally intense at the edges (acoustic Doppler current profiler (ADCP)-derived current velocities of  $>1 \text{ m s}^{-1}$  down to 500 m; Supplementary Fig. 6). At the time of the cruise, the eddy had reached its maturity phase (157–166 d, for a total lifetime of 278 d) with an average effective radius of  $84 \pm 3 \text{ km}$  and a tangential speed of  $1.49 \pm 0.02 \text{ m s}^{-1}$  (mean  $\pm$  s.d.,  $n = 10$ ), which aligns with previous observations of a lifetime between 6 and 12 months<sup>29</sup> and implies a substantial amount of time for microbial communities to adapt and thrive.

Backtracking the origin of the cyclonic eddy, we found that it originated west of the GS in February 2022, trapping cold shelf water originating from the Labrador Current, then forming a cold ring and travelling first eastward of the GS until the end of April before turning back westward, eventually merging with another eddy (here considered as the end of the eddy's life) (Supplementary Fig. 7 and Supplementary Video 1). The MAB above the shelf is known for high  $N_2$  fixation activity<sup>20,30–32</sup>. Shelf water trapped in eddies can extend the spatial range of these highly active diazotrophic communities. Despite the strong retention of the cyclonic eddy in its centre, the periphery at the surface

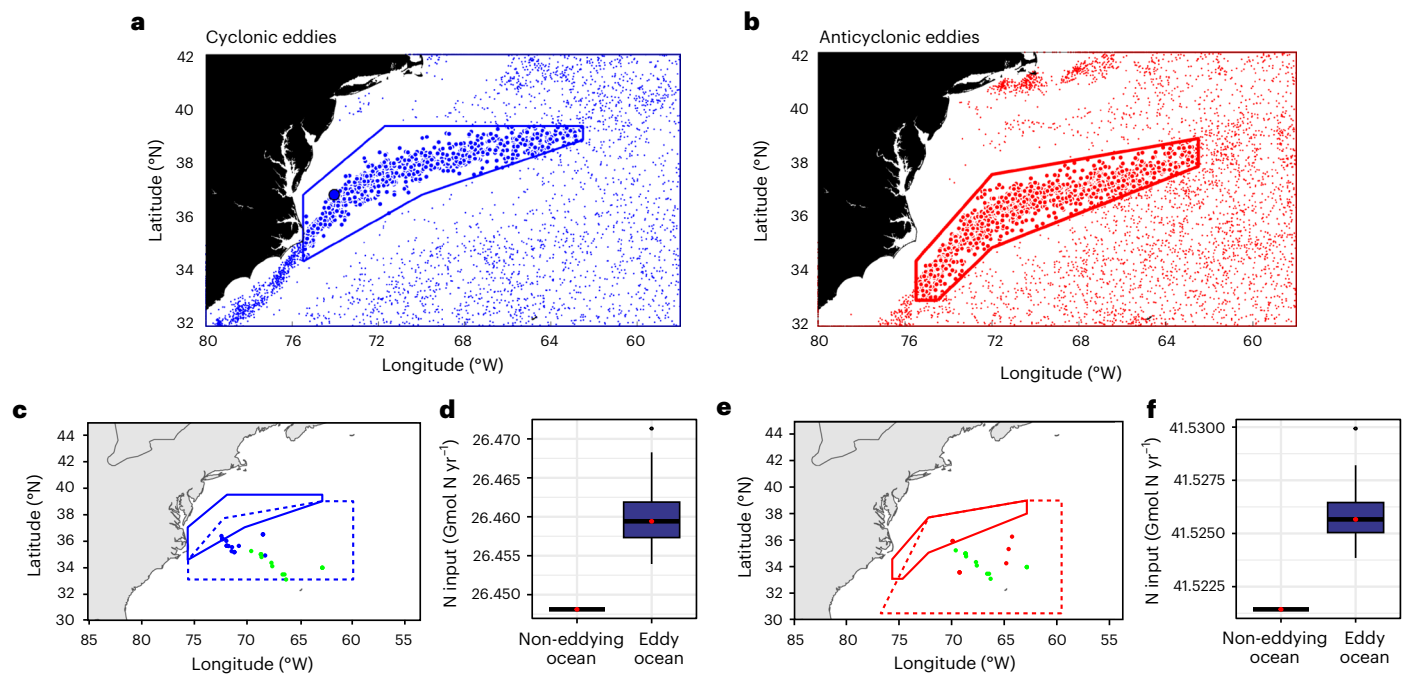


**Fig. 3 | Contribution of cyclonic and anticyclonic eddies to total  $N_2$  fixation in the western North Atlantic.** **a**, Cyclonic eddies detected using the NRT Eddy Atlas. Each dot corresponds to an eddy at its origin. Eddies inside the polygon have water masses of origin similar to that of the cyclonic eddy sampled during the FIGURE cruise (large blue dot), that is, west of the GS. **b**, Anticyclonic eddies detected using the Eddy Atlas. Eddies inside the polygon probably match the water mass of origin of the anticyclonic eddy sampled during the FIGURE cruise. **c**, In situ samples of  $N_2$  fixation within cyclonic eddies (blue dots) and  $N_2$  fixation outside mesoscale eddies (green dots); the dotted polygon represents the effect range of cyclonic eddies. **d**,  $\log(N$  input) from  $N_2$  fixation measurements inside cyclonic eddies and surrounding ocean (eddy ocean) and  $N_2$  fixation assuming

no mesoscale eddies inside the polygon (non-eddy ocean). **e**, In situ samples of  $N_2$  fixation within anticyclonic eddies (red dots) and  $N_2$  fixation outside mesoscale eddies (green dots); the dotted polygon represents the effect range of anticyclonic eddies. **f**,  $\log(N$  input) from  $N_2$  fixation measurements inside anticyclonic eddies and surrounding ocean (eddy ocean) and  $N_2$  fixation assuming no mesoscale eddies inside the polygon (non-eddy ocean). The box plots in **d** and **f** show distributions of each group of data points, including 58 data points from yearly averages, with data range indicated by upper and lower whiskers (maximum  $1.5 \times$  interquartile range, and outliers indicated by back dots) and 25% (box lower bound), median (box centre line and red dot) and 75% (box upper bound) percentiles. Basemap derived from <https://www.natureearthdata.com>.

can be subject to increased mixing. In this way, eddies contribute a large fraction of nutrient input into the North Atlantic Ocean<sup>33,34</sup>, which can support up to 20–30% of the primary production around Bermuda<sup>35</sup>. GS eddies have been linked to increased phosphorus input that can directly fuel  $N_2$  fixation<sup>32</sup>. Therefore, both mechanisms can be at play in our study, that is, eddy-driven seeding of diazotrophic organisms into surrounding waters and the dominance of better-adapted diazotrophs, particularly in the well-isolated core of the eddy.

### Physically coupled diazotroph community dynamics

The importance of physically modulated diazotroph distribution was supported by the dominance and asymmetric distribution of *Trichodesmium nifH* gene copy abundance (Fig. 2c–f). *Trichodesmium* have been recurrently observed in eddies<sup>36</sup>, as they disperse and accumulate in converging water masses due to their buoyancy<sup>37</sup>. Additionally, we consistently found numerous *nifH* gene copies of the non-cyanobacterial diazotroph Gamma A across the GS and the western edge of the cyclonic eddy. Although Gamma A has been previously observed in highly productive eddies<sup>38,39</sup>, its abundance decreased substantially towards the eddy's centre and its eastern edge in our measurements. Gamma A is comparable to a recently reported symbiont of a pennate diatom, with as yet little representation in the GS region<sup>40</sup>. The impact of fine scales on this association awaits exploration. UCYN-A1 *nifH* gene copies were consistently abundant across the GS with high copy numbers down to ~100 m (ST6), but vanished at the interface of the GS and the cyclonic eddy, except above the deep chlorophyll maximum at the eastern edge of the cyclonic eddy. Even though high nitrate concentrations suggest more favourable conditions for UCYN-A1 than for *Trichodesmium* within the cyclonic eddy<sup>41</sup>, the observed abundance gradient shows that

physical processes regulate diazotroph abundances through fast dilution, creation of suitable environments through, for example, elevated iron concentrations<sup>42</sup>, and/or competitive exclusion of GS-associated diazotrophs.

We used 16S rRNA gene sequencing as a genetic fingerprint to relate the diazotroph community to the extent of microbial community similarity between oceanographic structures<sup>43,44</sup>. All physically distinct structures also had unique genetic fingerprints (permutational analysis of variance, permutations = 999,  $R^2 = 0.22$ ,  $P < 0.001$ ;  $n = 41$ ; Supplementary Fig. 8). We could not find a higher similarity between the centre of the cyclonic eddy (ST2) and the MAB (ST8) when compared with other structures. This indicates that the time between the birth of the eddy and the time of sampling (~5 months after birth) was long enough for an eddy-specific community to adapt and thrive. We found a similar genetic fingerprint between the eastern edge of the cyclonic eddy and the centre of the anticyclonic eddy at 60–75 m depth, suggesting community connectivity between the eddies, which was also visible in the diazotrophic community using *nifH* gene sequencing (Supplementary Figs. 9 and 10). Similar connectivity between two counterrotating eddies has been observed in the Mediterranean Sea before<sup>45</sup>. This shows that the diazotroph community can be highly dynamic over time, which needs further investigation, particularly regarding community connectivity at the eddy–eddy interface and between eddy edges and ambient waters.

### Quantifying nitrogen input by $N_2$ fixation within eddies

Current  $N_2$  fixation measurements in the temperate western North Atlantic (defined here by the GS and GS eddy-influenced region between 30.35 and 39.00° N and 59.14 and 78.58° W; Supplementary

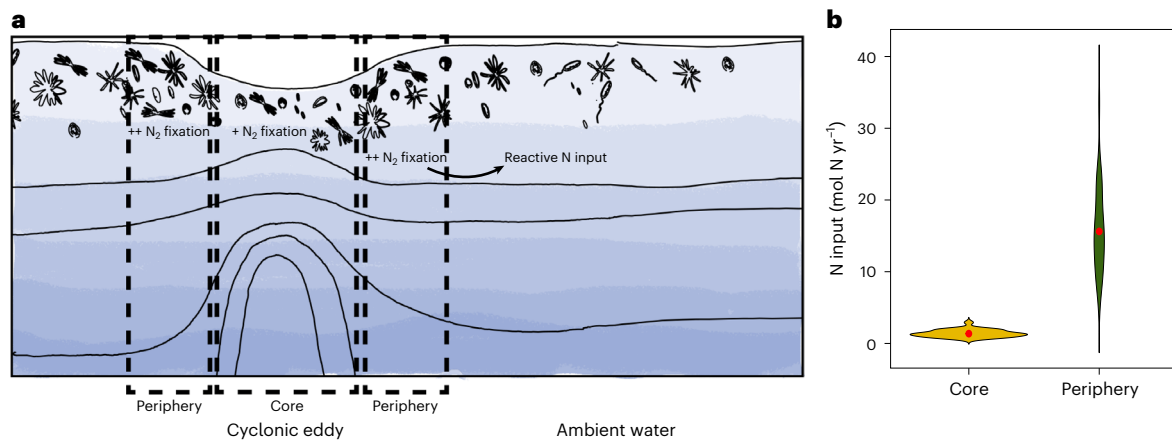


**Fig. 4 | Eddy edges play an important role in overall  $N_2$  fixation in mesoscale cyclonic eddies.** **a**, Conceptual representation of the strength of  $N_2$  fixation within a cyclonic eddy and its interaction with the ambient water.  $N_2$  fixation is highest at the edge of the cyclonic eddy, which is also where reactive nitrogen can be seeded in the ambient water. The separation between eddy core and

edge is based on Okubo–Weiss parameters ( $OW = 0$ ). **b**, Violin plot showing the distribution of N input from  $N_2$  fixation between the core and edge of cyclonic eddies ( $n = 58$ ). Width of the density curves correspond to frequency of nitrogen input measurements; median indicated by red dot.

Data 1) are primarily concentrated in the MAB, where rates are significantly higher (mean =  $32.54 \text{ nmol N l}^{-1} \text{ d}^{-1}$ ,  $n = 211$ ) than in the North Atlantic Gyre (mean =  $7.85 \text{ nmol N l}^{-1} \text{ d}^{-1}$ ,  $n = 57$ ; Welch  $t$ -test  $P < 0.001$ ). However, GS eddies could substantially extend the distribution of the productive organisms from the MAB into the North Atlantic Gyre. To provide a first-order estimate of eddy-borne nitrogen input by diazotrophs, we identified mesoscale eddies with similar water masses of origin using the NRT Eddy Atlas (Supplementary Data 2 and 3). Start polygons were selected according to underlying water mass similarities and seasons with the surveyed eddies (Fig. 3a,b). Extrapolating the impact of eddies that occurred between June and September resulted in an effect range of  $7.77 \times 10^{11} \text{ km}^2$  for cyclonic eddies and  $1.22 \times 10^{12} \text{ km}^2$  for anticyclonic eddies, where cyclonic eddies covered  $5.5 \times 10^{-6}\%$  and anticyclonic eddies  $2.61 \times 10^{-6}\%$  within their individual effect ranges (Fig. 3c,e). Integrated  $N_2$  fixation over 100 m depth within cyclonic eddies was 17 times higher than in ambient waters (Supplementary Table 2), contributing  $0.058 \pm 0.02\%$  to the total  $N_2$  fixation in the region when normalized to their effect range and assuming constant  $N_2$  fixation across the eddies' lifetime, or  $0.045\%$  when only considering the mature phase of eddies.  $N_2$  fixation within anticyclonic eddies contributed another  $0.014 \pm 0.004\%$  ( $0.011\%$  in the eddies' mature phase), with nine times higher rates in anticyclonic eddies than in ambient waters. In total,  $N_2$  fixation within eddies resulted in a total input of  $0.03403 \text{ mol N m}^{-2} \text{ yr}^{-1}$ , confirming previous quantifications based on phosphate input from Ekman advection into the North Atlantic Gyre<sup>23</sup>. However, we challenge the underlying mechanisms as we find important contributions from both cyclonic and anticyclonic eddies. Overall, this input could cover  $\sim 7.5\%$  of the total nitrate demand in the North Atlantic Gyre<sup>46</sup>, highlighting the role of mesoscale eddies as important vehicles for diazotrophic transport and activity in the North Atlantic Gyre.

We further attempted to integrate our observed differences between measurements at the edges and the centre of the cyclonic eddy in the calculations above. We found that the eddy edge accounts for  $\sim 92\%$  of the overall  $N_2$  fixation, but only covers  $\sim 83\%$  of the eddy volume (Fig. 4). Therefore,  $N_2$  fixation inputs from cyclonic eddies could be 1.6 times higher than if measurements were made in and extrapolated from the eddy core. Conversely, measurements could be 1.1 times overestimated when extrapolated from the eddy edge. Our results highlight the importance of the eddy edge for  $N_2$  fixation within mesoscale eddies, calling for more submesoscale measurements to determine an 'edge factor' when extrapolating  $N_2$  fixation measurements from mesoscale

eddies. Furthermore, as eddy edges are in direct contact with the ambient waters, they can fuel phytoplankton growth, extending the spatial range of eddy-influenced zones<sup>47</sup>.

As eddies become more frequent with climate change<sup>48,49</sup> and the GS is moving shoreward<sup>50</sup>, we estimated the sum of available similar summer anticyclonic and cyclonic eddies per decade from the NRT Eddy Atlas, and found a positive trend for the occurrence of anticyclonic eddies ( $+0.16 \pm 0.07$  eddies  $\text{yr}^{-1}$ ) while cyclonic eddies remained relatively stable ( $-0.03 \pm 0.05$  eddies  $\text{yr}^{-1}$ ). The positive trend of the occurrence of anticyclonic eddies could mean 2.3–3.2% more  $N_2$  fixation input from anticyclonic eddies per decade (calculated between 2011 and 2021). This increased input could potentially be an important balancing mechanism for increased desertification of the North Atlantic Gyre and associated increased nitrate demand in the future<sup>51</sup>.

## Conclusions

We show that cyclonic eddies are as important as anticyclonic eddies in supporting  $N_2$  fixation in the western North Atlantic Gyre. Furthermore, we identified the edges of cyclonic eddies as  $N_2$  fixation hotspots, with potential diazotroph community connectivity pathways into ambient waters. The recurrence of mesoscale eddies that transport highly active diazotroph communities from the MAB into the North Atlantic Gyre creates approximately 17 times higher  $N_2$  fixation rates in cyclonic eddies and 9 times higher  $N_2$  fixation rates in anticyclonic eddies than in the ambient water, contributing  $0.06\%$  to the total  $N_2$  fixation when eddies are considered coherent structures. We speculate that by resolving these inputs at the submesoscale this contribution could be even higher. As the activity of eddies may evolve with global warming<sup>48,49</sup>, their role in fertilizing the North Atlantic Gyre urgently needs to be integrated into global nitrogen budgets.

## Online content

Any methods, additional references, Nature Portfolio reporting summaries, source data, extended data, supplementary information, acknowledgements, peer review information; details of author contributions and competing interests; and statements of data and code availability are available at <https://doi.org/10.1038/s41561-024-01567-2>.

## References

- Wenegrat, J. O. et al. Enhanced mixing across the gyre boundary at the Gulf Stream front. *Proc. Natl Acad. Sci. USA* **117**, 17607–17614 (2020).

2. Lévy, M. et al. The impact of fine-scale currents on biogeochemical cycles in a changing ocean. *Annu. Rev. Mar. Sci.* **16**, 191–215 (2024).
3. Shao, Z. et al. Global oceanic diazotroph database version 2 and elevated estimate of global oceanic N<sub>2</sub> fixation. *Earth Syst. Sci. Data* **15**, 3673–3709 (2023).
4. Reynolds, S. E. et al. How widespread and important is N<sub>2</sub> fixation in the North Atlantic Ocean? *Glob. Biogeochem. Cycles* **21**, GB4015 (2007).
5. Chelton, D. B., Schlax, M. G., Samelson, R. M. & De Szoeko, R. A. Global observations of large oceanic eddies. *Geophys. Res. Lett.* **34**, L15606 (2007).
6. Behrenfeld, M. J. et al. Climate-driven trends in contemporary ocean productivity. *Nature* **444**, 752–755 (2006).
7. Lévy, M., Jahn, O., Dutkiewicz, S., Follows, M. J. & d'Ovidio, F. The dynamical landscape of marine phytoplankton diversity. *J. R. Soc. Interface* **12**, 20150481 (2015).
8. Liu, J. et al. Effect of mesoscale eddies on diazotroph community structure and nitrogen fixation rates in the South China Sea. *Reg. Stud. Mar. Sci.* **35**, 101106 (2020).
9. Church, M. J. et al. Physical forcing of nitrogen fixation and diazotroph community structure in the North Pacific subtropical gyre. *Glob. Biogeochem. Cycles* **23**, 2008GB003418 (2009).
10. Olson, E. M. et al. Mesoscale eddies and *Trichodesmium* spp. distributions in the southwestern North Atlantic. *J. Geophys. Res. Oceans* **120**, 4129–4150 (2015).
11. Guidi, L. et al. Does eddy–eddy interaction control surface phytoplankton distribution and carbon export in the North Pacific Subtropical Gyre? *J. Geophys. Res.* **117**, G2024 (2012).
12. Dugenne, M. et al. Nitrogen fixation in mesoscale eddies of the North Pacific Subtropical Gyre: patterns and mechanisms. *Glob. Biogeochem. Cycles* **37**, e2022GB007386 (2023).
13. Shiah, F.-K. et al. Viral shunt in tropical oligotrophic ocean. *Sci. Adv.* **8**, eabo2829 (2022).
14. Lehahn, Y. et al. Decoupling physical from biological processes to assess the impact of viruses on a mesoscale algal bloom. *Curr. Biol.* **24**, 2041–2046 (2014).
15. Gronniger, J. L., Gray, P. C., Niebergall, A. K., Johnson, Z. I. & Hunt, D. E. A Gulf Stream frontal eddy harbors a distinct microbiome compared to adjacent waters. *PLoS ONE* **18**, e0293334 (2023).
16. Robidart, J. C. et al. Effects of nutrient enrichment on surface microbial community gene expression in the oligotrophic North Pacific Subtropical Gyre. *ISME J.* **13**, 374–387 (2019).
17. Zehr, J. P. & Capone, D. G. Changing perspectives in marine nitrogen fixation. *Science* **368**, eaay9514 (2020).
18. Berman-Frank, I., Quigg, A., Finkel, Z. V., Irwin, A. J. & Haramaty, L. Nitrogen-fixation strategies and Fe requirements in cyanobacteria. *Limnol. Oceanogr.* **52**, 2260–2269 (2007).
19. Mulholland, M. R. et al. High rates of N<sub>2</sub> fixation in temperate, western North Atlantic coastal waters expand the realm of marine diazotrophy. *Glob. Biogeochem. Cycles* **33**, 826–840 (2019).
20. Mulholland, M. R. et al. Rates of dinitrogen fixation and the abundance of diazotrophs in North American coastal waters between Cape Hatteras and Georges Bank. *Limnol. Oceanogr.* **57**, 1067–1083 (2012).
21. Benavides, M. et al. Sinking *Trichodesmium* fixes nitrogen in the dark ocean. *ISME J.* **16**, 2398–2405 (2022).
22. Benavides, M. et al. Fine-scale sampling unveils diazotroph patchiness in the South Pacific Ocean. *ISME Commun.* **1**, 3 (2021).
23. Palter, J. B., Lozier, M. S., Sarmiento, J. L. & Williams, R. G. The supply of excess phosphate across the Gulf Stream and the maintenance of subtropical nitrogen fixation. *Glob. Biogeochem. Cycles* **25**, GB4007 (2011).
24. Carracedo, L. I. et al. CARING cruise biogeochemical data (nutrients, pH, total alkalinity, pCO<sub>2</sub>). *SEANOE* <https://doi.org/10.17882/96728> (2022).
25. Holl, C. M. & Montoya, J. P. Interactions between nitrate uptake and nitrogen fixation in continuous cultures of the marine diazotroph *Trichodesmium* (Cyanobacteria). *J. Phycol.* **41**, 1178–1183 (2005).
26. Lu, Y. et al. Biogeography of N<sub>2</sub> fixation influenced by the western boundary current intrusion in the South China Sea. *J. Geophys. Res.* **124**, 6983–6996 (2019).
27. Jiang, Z. et al. Enhancement of summer nitrogen fixation by the Kuroshio Intrusion in the East China Sea and Southern Yellow Sea. *J. Geophys. Res.* **128**, e2022JG007287 (2023).
28. Pegliasco, C. et al. META3.1exp: a new global Mesoscale Eddy Trajectory Atlas derived from altimetry. *Earth Syst. Sci. Data* **14**, 1087–1107 (2022).
29. The Ring Group. Gulf Stream cold-core rings: their physics, chemistry, and biology. *Science* **212**, 1091–1100 (1981).
30. Selden, C. R. et al. A coastal N<sub>2</sub> fixation hotspot at the Cape Hatteras front: elucidating spatial heterogeneity in diazotroph activity via supervised machine learning. *Limnol. Oceanogr.* **66**, 1832–1849 (2021).
31. Tang, W., Li, Z. & Cassar, N. Machine learning estimates of global marine nitrogen fixation. *J. Geophys. Res.* **124**, 717–730 (2019).
32. Palter, J. B. et al. High N<sub>2</sub> fixation in and near the Gulf Stream consistent with a circulation control on diazotrophy. *Geophys. Res. Lett.* **47**, e2020GL089103 (2020).
33. McGillicuddy, D. J. & Robinson, A. R. Eddy-induced nutrient supply and new production in the Sargasso Sea. *Deep-Sea Res. I* **44**, 1427–1450 (1997).
34. McGillicuddy, D. J., Anderson, L. A., Doney, S. C. & Maltrud, M. E. Eddy-driven sources and sinks of nutrients in the upper ocean: results from a 0.1° resolution model of the North Atlantic. *Glob. Biogeochem. Cycles* **17**, 2002GB001987 (2003).
35. Jenkins, W. J. & Goldman, J. C. Seasonal oxygen cycling and primary production in the Sargasso Sea. *J. Mar. Res.* **43**, 465–491 (1985).
36. Davis, C. S. & McGillicuddy, D. J. Transatlantic abundance of the N<sub>2</sub>-fixing colonial cyanobacterium *Trichodesmium*. *Science* **312**, 1517–1520 (2006).
37. Eichner, M., Inomura, K., Pierella Karlusich, J. J. & Shaked, Y. Better together? Lessons on sociality from *Trichodesmium*. *Trends Microbiol.* **31**, 1072–1084 (2023).
38. Shao, Z. & Luo, Y.-W. Controlling factors on the global distribution of a representative marine non-cyanobacterial diazotroph phylotype (Gamma A). *Biogeosciences* **19**, 2939–2952 (2022).
39. Fong, A. A. et al. Nitrogen fixation in an anticyclonic eddy in the oligotrophic North Pacific Ocean. *ISME J.* **2**, 663–676 (2008).
40. Tschitschko, B. et al. Rhizobia–diatom symbiosis fixes missing nitrogen in the ocean. *Nature* **630**, 899–904 (2024).
41. Mills, M. M. et al. Unusual marine cyanobacteria/haptophyte symbiosis relies on N<sub>2</sub> fixation even in N-rich environments. *ISME J.* **14**, 2395–2406 (2020).
42. Conway, T. M., Palter, J. B. & De Souza, G. F. Gulf Stream rings as a source of iron to the North Atlantic subtropical gyre. *Nat. Geosci.* **11**, 594–598 (2018).
43. Agogue, H., Lamy, D., Neal, P. R., Sogin, M. L. & Herndl, G. J. Water mass-specificity of bacterial communities in the North Atlantic revealed by massively parallel sequencing. *Mol. Ecol.* **20**, 258–274 (2011).
44. Djurhuus, A., Boersch-Supan, P. H., Mikalsen, S.-O. & Rogers, A. D. Microbe biogeography tracks water masses in a dynamic oceanic frontal system. *R. Soc. Open Sci.* **4**, 170033 (2017).
45. Belkin, N. et al. Influence of cyclonic and anticyclonic eddies on plankton in the southeastern Mediterranean Sea during late summertime. *Ocean Sci.* **18**, 693–715 (2022).

46. Dunne, J. P., Sarmiento, J. L. & Gnanadesikan, A. A synthesis of global particle export from the surface ocean and cycling through the ocean interior and on the seafloor. *Glob. Biogeochem. Cycles* **21**, 2006GB002907 (2007).
47. Lehahn, Y., d'Ovidio, F. & Koren, I. A satellite-based Lagrangian view on phytoplankton dynamics. *Annu. Rev. Mar. Sci.* **10**, 99–119 (2018).
48. Beech, N. et al. Long-term evolution of ocean eddy activity in a warming world. *Nat. Clim. Change* **12**, 910–917 (2022).
49. Martínez-Moreno, J. et al. Global changes in oceanic mesoscale currents over the satellite altimetry record. *Nat. Clim. Change* **11**, 397–403 (2021).
50. Todd, R. E. & Ren, A. S. Warming and lateral shift of the Gulf Stream from in situ observations since 2001. *Nat. Clim. Change* **13**, 1348–1352 (2023).
51. Leonelli, F. E. et al. Ultra-oligotrophic waters expansion in the North Atlantic Subtropical Gyre revealed by 21 years of satellite observations. *Geophys. Res. Lett.* **49**, e2021GL096965 (2022).

**Publisher's note** Springer Nature remains neutral with regard to jurisdictional claims in published maps and institutional affiliations.

**Open Access** This article is licensed under a Creative Commons Attribution 4.0 International License, which permits use, sharing, adaptation, distribution and reproduction in any medium or format, as long as you give appropriate credit to the original author(s) and the source, provide a link to the Creative Commons licence, and indicate if changes were made. The images or other third party material in this article are included in the article's Creative Commons licence, unless indicated otherwise in a credit line to the material. If material is not included in the article's Creative Commons licence and your intended use is not permitted by statutory regulation or exceeds the permitted use, you will need to obtain permission directly from the copyright holder. To view a copy of this licence, visit <http://creativecommons.org/licenses/by/4.0/>.

© The Author(s) 2024

<sup>1</sup>Ecological Chemistry, Alfred-Wegener-Institut Helmholtz-Zentrum für Polar- und Meeresforschung, Bremerhaven, Germany. <sup>2</sup>Aix Marseille Université, Université de Toulon, CNRS, IRD, MIO UM 110, Marseille, France. <sup>3</sup>Turing Centre for Living Systems, Aix-Marseille University, Marseille, France. <sup>4</sup>ECOQUA, Universidad de Las Palmas de Gran Canaria, Las Palmas de Gran Canaria, Spain. <sup>5</sup>Unidad Océano y Clima, Instituto de Oceanografía y Cambio Global (IOCAG), Universidad de Las Palmas de Gran Canaria (ULPGC), Unidad Asociada ULPGC-CSIC, Las Palmas de Gran Canaria, Spain. <sup>6</sup>Laboratoire d'Océanographie Physique et Spatiale (LOPS), IUEM, University of Brest, CNRS, Ifremer, IRD, Plouzané, France. <sup>7</sup>National Oceanography Centre, European Way, Southampton, UK. ✉ e-mail: [cora.hoerstmann@awi.de](mailto:cora.hoerstmann@awi.de); [borja.aguiar@ulpgc.es](mailto:borja.aguiar@ulpgc.es); [mar.benavides@noc.ac.uk](mailto:mar.benavides@noc.ac.uk)

## Methods

### Sampling campaign

Data and samples were collected during the Eurofleets+FIGURE-CARING research campaign (<https://doi.org/10.17600/18002940>), performing a transect across an anticyclonic eddy, a cyclonic eddy and the GS (Fig. 1) between 21 and 30 July 2022 on board RV Atlantic Explorer (cruise AE2215).

### Physical oceanography

An adjusted cruise track led by real-time information from the software package SPASSO (<https://spasso.mio.osupytheas.fr>)<sup>52,53</sup> allowed us to follow the targeted eddies and the respective boundary region of the GS. Observations were made between 12 May and 12 December 2022 to follow the evolution of the eddies. At each station, conductivity, temperature and depth profiles were obtained using an SBE9 CTD (Sea-Bird Electronics) and an SBE11+ deck unit. The CTD carried a variety of additional sensors including a dissolved oxygen sensor, transmissometer, fluorometer, photosynthetic active radiation sensor, altimeter, digital reversing thermometer and bottom-contact switch. In conjunction with a modified SBE Rosette frame, the CTD system utilized a SBE32 full-size carousel water sampler, equipped with 24 Niskin-type 12 l bottles attached to the frame. We examined temperature–salinity profiles and interpolated temperature, salinity, oxygen and fluorescence longitudinally across our transect using a modification<sup>54</sup> of the ggplot2 PlotSvalbard extension (<https://github.com/MikkoVihtakari/PlotSvalbard>) in R (v.4.2.2). Additionally, we characterized the sea surface temperature of the cyclonic eddy and ambient waters using the OSTIA L4 product from the C3S project, produced using the OSTIA reanalysis system v3.1<sup>55</sup> and adjacent Argo floats (<https://dataselection.euro-argo.eu/>). Satellite sea surface height was derived from AVISO (<https://www.aviso.altimetry.fr/en/data/products/sea-surface-height-products.html>). Finally, we also took into account pathways of adjacent drifters, which are from the Global Drifter Program (<https://www.aoml.noaa.gov/phod/gdp/index.php>).

### Dissolved inorganic nutrients

Discrete water samples (30 ml plastic flasks) were collected from the Niskin bottles for inorganic nutrients (nitrate, phosphate and silicate). Samples were pasteurized while on board and analysed at IRD/IMAGO (Ifremer) with an AAIII Seal-Analytical auto-analyser, following the protocol established by IMAGO (certified ISO 9001:2015)<sup>56</sup>. The precision for nitrate, phosphate and silicate was evaluated as 0.027, 0.004 and 0.035  $\mu\text{mol kg}^{-1}$ , respectively. We calculated  $P^*$  as an estimate for excess phosphate according to the Redfield ratio<sup>57</sup>.

### Fine-scale structure identification

The eddies and the GS were localized before and during the cruise using SPASSO's plotting and diagnostics (geostrophic currents, sea surface temperature, chlorophyll, Okubo–Weiss and FSLE<sup>58</sup>). Each sampling site is qualitatively classified mainly using ADCP measurements, completed by surface temperature and salinity. The direction and intensity of the ADCP currents are used to define the rotational direction of the eddies. Crossing the eddies from the edges to the core, the maximal tangential current intensity showed a linear increase at the eddy's edges and a linear decrease towards the eddy core. The anticyclonic eddy shows a low-temperature and high-salinity core (ST0). The cyclonic eddy shows a low-temperature and low-salinity core (ST2). The GS is identified with a very high current intensity, as well as high temperature and salinity (ST6). ST8 in the MAB shows a low current intensity, as well as low temperature and salinity.

### Identification of eddy origin

The mesoscale eddy activity was studied on the basis of META3.0exp NRT. This atlas covers the period from 1 January 2018 to the present, and was produced by SSALTO/DUACS and distributed by AVISO+

(<https://www.aviso.altimetry.fr/>) with support from CNES and in collaboration with IMEDEA. Further details of the eddy tracking algorithm can be found in ref. 59.

The NRT Eddy Atlas enabled the backtracking of the cyclonic eddy surveyed during the cruise; however, the origin of the anticyclonic eddy is unclear and it is absent from the NRT Eddy Atlas. We can use the NRT Eddy Atlas to investigate the historical database and geometric properties of eddies with an origin associated with the surroundings of the GS on the basis of META3.1exp DT. This atlas covers the period from 1 January 1993 to 7 March 2020. It was produced by SSALTO/DUACS and distributed by AVISO+ (<https://www.aviso.altimetry.fr>) with support from CNES, in collaboration with IMEDEA (<https://doi.org/10.24400/527896/a01-2021.001> for the META3.1exp DT allsat version).

### Identification of similar eddies in the study region

First, we defined an exact grid of our study region. We set the study region on the basis of water masses of origin for cyclonic eddies, being limited in the south down to Cape Hatteras, which is roughly the extent of the southward flowing Labrador Current. In the north, we used the turn and, therefore, changes in the characteristics of the GS as a boundary. We then identified all eddies within this grid.

The effect ranges east of the GS of cyclonic and anticyclonic eddies were calculated using the maximum latitudinal and longitudinal endpoints of eddies derived from the NRT Eddy Atlas as the northern, southern and eastern boundaries and the GS (as above) as the western boundary.

To derive eddies that only occurred during the summer season, we removed eddies that disappeared before June and originated after September from our analysis, resulting in 313 cyclonic eddies and 422 anticyclonic eddies between 1993 and 2022 (average  $11 \pm 3$  cyclonic eddies  $\text{yr}^{-1}$  and  $15 \pm 2$  anticyclonic eddies  $\text{yr}^{-1}$ ). In this work we used the shipboard ADCP vertical profiles collected during the cruise and the altimeter-derived propagation speed of the eddies to compute their nonlinearity ratio. Accounting for rotational speeds well above 20  $\text{cm s}^{-1}$  and 40  $\text{cm s}^{-1}$  down to 700 m depth for the anticyclonic and cyclonic eddies (Supplementary Fig. 11), and mean propagation speeds of about 4.2  $\text{cm s}^{-1}$  and 6.6  $\text{cm s}^{-1}$  (Supplementary Data 2 and 3), respectively, their nonlinearity ratios indicate that these eddies have abilities to transport ocean properties at least down to 700 m while propagating (Supplementary Fig. 12). As a conservative approach, we used 100 m depth to calculate the eddy volume, which also matches our  $\text{N}_2$  fixation sampling depth. We calculated the regression of eddies per year to derive a trend of the frequency of eddies per year. The s.d. from the linear regression was calculated on the basis of sample residuals.

### Differentiation between eddy core and periphery

We used the distance between the sampled cyclonic eddy core and the distance to the point where the Okubo–Weiss parameter is equal to 0 to identify the transition zone between the eddy core and edge. We identified the radius of the eddy core using the `dism()` function of the geosphere package (v.1.5.18) in R. This resulted in a radius of 36.7 km out of 87.9 km total radius (Supplementary Fig. 12).

### $\text{N}_2$ fixation rate measurements

At each CTD station, we took triplicate water samples to measure  $\text{N}_2$  fixation from three depths (ST0) or four depths (ST1, ST2, ST3, ST6 and ST8). All incubation bottles (2.25 l and 4.25 l) were rinsed before sampling with 10% HCl, deionized water and sampling water. Samples were spiked with 98%  $^{15}\text{N}_2$  gas (Eurisotop, lot number 29/062001) and incubated in shaded deck incubators for 24 h. We used the dissolution method<sup>60</sup>. In brief, we added a 2 ml gas bottle to 2.25 l bottles and 4 ml to 4.25 l bottles; 2.25 l bottles were stirred on a magnetic plate for 4 min and 4.25 l bottles were shaken by hand for 4 min. After bubble dissolution, bottles were briefly opened to remove the magnetic stirrer and the remaining bubble to avoid further equilibration between the gas



and aqueous phase. After incubation, for each sample, a subsample for membrane inlet mass spectrometry analyses was transferred to a 12 ml Exetainer, and the remaining content was filtered onto 25 mm precombusted GFF filters and stored at  $-20^{\circ}\text{C}$  while at sea. Additionally, 4 l of water samples was directly filtered onto precombusted GFF filters and used for natural  $^{15}\text{N}/^{14}\text{N}$  ratio measurements. We quantified the  $^{15}\text{N}$  atom% enrichment of PN using an elemental analyser connected with an isotope ratio mass spectrometer (Integra2, Sercon). The isotope ratio mass spectrometer was calibrated using IAEA reference material IAEA-600. Membrane inlet mass spectrometry analyses were carried out according to ref. 61.  $\text{N}_2$  fixation rates were calculated according to ref. 62. The minimum quantifiable rate with exact error propagation was calculated<sup>63</sup> (Supplementary Data 4). We calculated the average  $\text{N}_2$  fixation of triplicates and plotted it against FSLE and interpolated longitudinal temperature section using the *plotly* package (v.4.10.1) in R to identify  $\text{N}_2$  fixation in relation to oceanographic structures.

### $\text{N}_2$ extrapolation on the basis of mesoscale eddies

**Classification of previous  $\text{N}_2$  fixation measurements in mesoscale eddies in the study region.** We compiled previous measurements in the region affected by similar GS eddies (see ‘Identification of similar eddies in the study region’) and grouped them into eddy-affected samples: cyclonic eddies, anticyclonic eddies, open ocean and samples in the MAB. Specifically, we retrieved  $\text{N}_2$  fixation data from the global diazotrophic database version 2 (ref. 3) and mapped those samples against sea surface altimetry (sea-level anomaly, SLA) satellite products (Copernicus Marine Data, processed by the DUACS multimission altimeter data processing system; <https://doi.org/10.48670/moi-00148>), with a date range selection of a maximum of 15 d per individual dataset. This resulted in 316 samples between 0 and 100 m depth in 17 different SLA bins between 2007 and 2022, when our cruise took place (Supplementary Data 1). Samples were visually inspected and classified as eddies if a clear circular SLA anomaly was visible.

**Extrapolation of nitrogen input from  $\text{N}_2$  fixation in eddies.** We took a conservative approach to calculate the average eddy-borne  $\text{N}_2$  fixation input to the North Atlantic Gyre. We extrapolated  $\text{N}_2$  fixation rates measured in cyclonic and anticyclonic eddies from this study and previous studies (Supplementary Data 1) to the number of eddies of similar water mass origin generated during summer months within the area covering their birth, maturation and death using the NRT Eddy Atlas (dashed lines in Fig. 3c–e):

$$\begin{aligned} \text{N input(eddies)} \\ = \text{mean}(\text{N}_2 \text{ fixation}) \times \text{volume(eddies)} \times \text{lifetime(eddies)} \times n \end{aligned} \quad (1)$$

taking the arithmetic mean from  $\text{N}_2$  fixation in nanomoles of N per metre cubed per day, eddy volume in metres cubed, eddy lifetime in days and the number of eddies ( $n$ ).

Notably, measurements in the region are largely restricted to summer months. Therefore, calculations in this study are limited to eddies between June and September.

Eddy properties substantially change between the birth and decay phases<sup>64</sup>. Therefore, we additionally provide  $\text{N}_2$  fixation input estimates only considering the mature phase (80% of the eddies’ lifetime<sup>64</sup>), where eddy properties are most stable and match our sample measurements.

The background average  $\text{N}_2$  fixation input was calculated from previous studies in the region (Supplementary Data 1) and extrapolated to the study grid (Fig. 3c–e), subtracting the area covered by eddies.

The sampling spatial resolution in eddies from previous studies is too low to distinguish core from edge. Hence, to calculate the over- or underestimation of  $\text{N}_2$  fixation depending on the sample location (core/ edge), we only considered our own dataset, which had a sampling spatial resolution of  $\sim 30$  km, allowing us to distinguish core from edge  $\text{N}_2$  fixation and diazotroph communities.

Relative additional  $\text{N}_2$  fixation input from increasing eddy activity within a decade was calculated between 2011 and 2021 using the linear regression for increasing anticyclonic eddy activity. The lower bound was calculated using the mean from the beginning until the mid-decade and from the mid-decade until the end of the decade. The upper bound of percentage additional input was calculated between 2011 and 2021 using the difference between the N input from eddies in comparison with the ambient water, normalized by the mean eddy lifetime (per year).

### Diazotrophic and prokaryotic diversity

**DNA sampling and nucleic acid extraction.** At each station, we took around 4.25 l seawater samples from the Niskin bottles (depth-resolved CTD stations) or of the ships’ underway seawater pump (surface underway samples). Samples were filtered onto  $0.2 \mu\text{m}$  Supor filters (Pall) with a peristaltic pump. Filters were transformed into sterile bead beater tubes, and  $50 \mu\text{l}$  RNAlater (Fisher Scientific) was added to stabilize the samples for transport. Tubes were flash-frozen in liquid nitrogen and kept at  $-80^{\circ}\text{C}$  until extraction. DNA was extracted using the DNeasy Plant Mini Kit (Qiagen), with an additional step of proteinase K treatment after sample bead beating. In brief, we added  $50 \mu\text{l}$  proteinase K (Qiagen) to each tube and incubated the samples at  $55^{\circ}\text{C}$  for 2 h. We then continued normally with the DNase treatment following the manufacturer’s instructions. After DNA extraction, DNA concentration was quantified using a Varioskan and PicoGreen double-stranded DNA quantitation kit.

**qPCR counts.** *NifH* gene copies for *Trichodesmium*, UCYN-A1 and Gamma A were quantified with TaqMan qPCR assays on a CFX Opus Dx real-time PCR detection system (Bio-Rad) v.5.3.022.1030. We used the following primer and probes for the individual targeted taxa. For *Trichodesmium* we used forward primer 5’-GAC GAA GTA TTG AAG CCA GGT TTC-3’, reverse primer 5’-CGG CCA GCG CAA CCT A-3’ and probe 5’-FAM-CAT TAA GTG TGT TGA ATC TGG TGG TCC TGA GC-3’-TAMRA-3’ (ref. 65). For UCYN-A1 we used forward primer 5’-GGCTATAACAACGTTTTATGCGTTGA-3’, reverse primer 5’-ACCACGACCAGCACATCCA-3’ and probe 5’-FAM-TCCGGTGGTCTGAGCCTGGA-3’-TAMRA-3’ (ref. 65). For Gamma A we used forward 5’-CGG TAG AGG ATC TTG AGC TTG AA-3’, reverse 5’-CACCTGACTCCACGCACTTG-3’ and probe 5’-FAM-AAG TGC TTA AGG TTG GCT TTG GCG ACA-3’-TAMRA-3’ (ref. 66). Each reaction ( $12.5 \mu\text{l}$ ) consisted of  $6.125 \mu\text{l}$  TaqMan PCR Master Mix (Applied Biosystems),  $0.5 \mu\text{l}$  of the forward and reverse primers ( $10 \mu\text{M}$ ),  $0.25 \mu\text{l}$  probe ( $10 \mu\text{M}$ ),  $4 \mu\text{l}$  molecular biology grade water (Fisher BioReagents),  $0.125 \mu\text{l}$  BSA ( $10.08 \mu\text{g} \mu\text{l}^{-1}$ ) and  $1 \mu\text{l}$  standard or sample (samples were prediluted to  $2 \text{ng} \mu\text{l}^{-1}$  to add  $2 \text{ng}$  DNA to all qPCR reactions). The qPCR programme consisted of  $50^{\circ}\text{C}$  for 2 min, then  $95^{\circ}\text{C}$  for 10 min, followed by 45 cycles of  $95^{\circ}\text{C}$  for 30 s and  $60^{\circ}\text{C}$  for 1 min. Negative controls and standard dilutions from linearized plasmids containing the relevant *nifH* targets (accession number for *Trichodesmium*, AY528677; accession number for UCYN-A1, AF059642.1; accession number for Gamma A, EU052413). Standards ranged from  $10^1$  to  $10^7$  gene copies  $\text{l}^{-1}$  and were run in duplicate samples. No-template controls did not show any amplification. The qPCR efficiency ranged from 90 to 99%.

***nifH* gene and 16S rRNA gene library preparation and sequencing.** PCR products were generated for amplicon sequencing targeting the *nifH* gene, which serves as a functional marker for diazotrophic organisms, and variable region 4 (V4) of the prokaryotic 16S rRNA gene. We PCR amplified the ( $\sim 359$ -base-pair, bp) *nifH* gene from DNA extracts using a nested PCR protocol<sup>67,68</sup>. Hereby, two sets of degenerate primers were used, with the second set of primers nested within the first PCR products. Each sample was run in triplicate and pooled at the end of the nested PCR. The first PCR reaction included the *nifH3* reverse primer (5’-ATRTTRTTNGCNGCRTA-3’) and the *nifH4* forward primer

(5'-TTYTAYGGNAARGGNGG-3'). The second PCR reaction was done with the *nifH1* forward primer (5'-TGYGAYCCNAARGCNGA-3') and the *nifH2* reverse primer (5'-ADNGCCATCATYTCNCC-3'), which also carried the Illumina adaptors for further library preparation. PCR amplification targeting the V4 region of the 16S rRNA gene was performed using the 515F forward primer (5'-GTGYCAGCMGCCGCGGTAA-3')<sup>69</sup> and the 806R reverse primer (5'-GGACTACNVGGGTWTCTAAT-3')<sup>70</sup> as recommended by the Earth Microbiome Project (<https://earthmicrobiome.org/>). Each primer also carried Illumina-specific adaptors for downstream library preparation. PCR products were generated with 50 µl of total reaction volume containing 22 µl PCR grade water, 10 µl MyTaq polymerase, 1 µl of each forward and reverse primer (10 µM), 2.5 µl MgCl<sub>2</sub> (25 mM), 1 µl BSA (10 mg ml<sup>-1</sup>) and 12 µl DNA template that was previously normalized to 2 ng µl<sup>-1</sup>. PCR cycles were run following standard protocols of amplicon library preparation (16S Metagenomic Sequencing Library Preparation, Illumina, part 15044223 Rev. B). All PCR products were cleaned using the MP Biomedicals GeneClean Turbo Kit and normalized to 25 ng µl<sup>-1</sup>. Normalized PCR products were submitted to Azenta GENEWIZ for subsequent library preparation and amplicon sequencing. *NifH* gene and 16S rRNA gene amplicon reads were generated using 300-bp paired-end sequencing with an Illumina NextSeq sequencer.

**Amplicon sequence variant (ASV) generation and taxonomic assignment.** Raw sequences were imported and processed in R (v.4.2.2) and RStudio (v.2023.06.0 + 421). We used the DADA2 (v.1.26.0) pipeline to process raw sequences into ASVs<sup>71</sup>. Primers were removed using cutadapt (v.4.3). The parameters in DADA2 were set as follows: truncLen = c(200, 180), maxN = 0, maxEE = c(2, 2), truncQ = 2, m.phix = TRUE. Denoised reads were merged using the function mergePairs(), and chimaeric contigs were removed with removeBimeraDenovo(). Taxonomic ranks for ASVs generated from *nifH* sequences were assigned using the *nifH* database tailored for the DADA2 pipeline (v.2.0.5)<sup>72</sup> and the assignTaxonomy() function. Taxonomic ranks for ASVs generated from 16S sequences were assigned using the Silva v.138.1 database for DADA2<sup>73</sup>.

### Statistical and community connectivity analyses

All statistical analyses were performed in R (v.4.4.0) and RStudio (v.2024.04.0 + 735). We tested differences in N<sub>2</sub> fixation between the physically classified fine-scale structures ('Classification of previous N<sub>2</sub> fixation measurements into mesoscale eddies in the study region') with analysis of variance for sample variances, followed by a two-sample *t*-test comparing individual structures using the stats package (v.4.4.0). We tested differences between N<sub>2</sub> fixation in different oceanographic structures within our study area (MAB–North Atlantic Gyre separated by the GS, and no eddy influences—eddy influences as identified using the Eddy Atlas) in the western North Atlantic with an *F*-test for sample variance followed by a Welch *t*-test. Due to the compositionality of sequencing data, we centred log-ratio (CLR)-transformed the *nifH* and 16S rRNA gene ASV tables. Before transformations, we removed all ASVs with only one instance across all samples and applied Bayesian-multiplicative treatments of zeros in the ASV tables using the cmultRepl() function of the zComposition package (v.1.5.0.3) to reduce the effect of zero-count samples. We examined the diazotrophic (*nifH*) and prokaryotic (16S) beta diversity structure by simple principal component analysis of the CLR-transformed ASV tables using the ordinate() and plot\_ordination() functions in phyloseq (v.1.48.0)<sup>74</sup>. Further, we explored the effect of environmental variables on the diazotrophic beta diversity structure by first performing a stepwise permutational analysis using the ordiR2step() function in vegan (v.2.6.4), followed by redundancy analysis including the significant explanatory variables derived from the permutational analysis as explanatory variables in our redundancy analysis. Differences of diazotrophic dissimilarity between oceanographic structures were tested with a permutational analysis of variance<sup>75</sup> on Aitchison of the *nifH* ASV table using the adonis2()

function in vegan (v.2.6.4). We compared sample similarity of *nifH* and 16S rRNA gene sequences by hierarchically clustering both ASV tables individually using the ward2 method of the hclust() function, followed by the as.dendrogram() function of the stats package (v.4.4.0), and mapped them against each other using the untangle() and tanglegram() functions of the dendextend package (v.1.17.1).

### Data availability

Source data are publicly available in the following databases: CTD data on the European Marine Observation and Data Network (EMODnet) UUID 538df51a-45d3-4380-9106-027ab5dd99b4; meteorological, navigation and underway data on EMODnet UUID 117ebd65-d4e1-46b1-ae5e-b0828d61ee1c. Nutrient data are publicly available under <https://doi.org/10.17882/96728>. Raw nitrogen fixation data are on SEANO <https://www.seano.org/data/00825/93650/>; *nifH* and 16S rRNA gene sequences are deposited in ENA under the project accession number PRJEB64428.

### Code availability

Code is publicly available under CoraHoerstmann/FIESTA: v2.0 in Zenodo<sup>54</sup>.

### References

- Doglioli, A. M. et al. A software package and hardware tools for in situ experiments in a Lagrangian reference frame. *J. Atmos. Ocean. Technol.* **30**, 1940–1950 (2013).
- Rousselet, L., Doglioli, A. M., Maes, C., Blanke, B. & Petrenko, A. A. Impacts of mesoscale activity on the water masses and circulation in the Coral Sea. *J. Geophys. Res.* **121**, 7277–7289 (2016).
- Hoerstmann, C. FIGURE code v2.0. Zenodo <https://doi.org/10.5281/zenodo.13477233> (2024).
- Merchant, C. J. et al. Satellite-based time-series of sea-surface temperature since 1981 for climate applications. *Sci. Data* **6**, 223 (2019).
- Aminot, A. & Kérouel, R. *Dosage Automatique des Nutriments dans les Eaux Marines. Méthodes en Flux Continué* (Ifremer-Quae, 2007).
- Deutsch, C., Sarmiento, J. L., Sigman, D. M., Gruber, N. & Dunne, J. P. Spatial coupling of nitrogen inputs and losses in the ocean. *Nature* **445**, 163–167 (2007).
- d'Ovidio, F. et al. The biogeochemical structuring role of horizontal stirring: Lagrangian perspectives on iron delivery downstream of the Kerguelen Plateau. *Biogeosciences* **12**, 5567–5581 (2015).
- Mason, E., Pascual, A. & McWilliams, J. C. A new sea surface height-based code for oceanic mesoscale eddy tracking. *J. Atmos. Ocean. Technol.* **31**, 1181–1188 (2014).
- Klawonn, I. et al. Simple approach for the preparation of <sup>15</sup>N<sub>2</sub>-enriched water for nitrogen fixation assessments: evaluation, application and recommendations. *Front Microbiol.* **6**, 769 (2015).
- Kana, T. M. et al. Membrane inlet mass spectrometer for rapid high-precision determination of N<sub>2</sub>, O<sub>2</sub>, and Ar in environmental water samples. *Anal. Chem.* **66**, 4166–4170 (1994).
- Montoya, J. P., Voss, M., Kahler, P. & Capone, D. G. A simple, high-precision, high-sensitivity tracer assay for N<sub>2</sub> fixation. *Appl. Environ. Microbiol.* **62**, 986–993 (1996).
- Gradoville, M. R. et al. Diversity and activity of nitrogen-fixing communities across ocean basins. *Limnol. Oceanogr.* **62**, 1895–1909 (2017).
- Pegliasco, C., Chaigneau, A. & Morrow, R. Main eddy vertical structures observed in the four major Eastern Boundary Upwelling systems. *J. Geophys. Res. Oceans* **120**, 6008–6033 (2015).

65. Church, M. J., Jenkins, B. D., Karl, D. M. & Zehr, J. P. Vertical distributions of nitrogen-fixing phylotypes at Stn ALOHA in the oligotrophic North Pacific. *Aquat. Microb. Ecol.* **38**, 3–14 (2005).
66. Moisaner, P. H., Beinart, R. A., Voss, M. & Zehr, J. P. Diversity and abundance of diazotrophic microorganisms in the South China Sea during intermonsoon. *ISME J.* **2**, 954–967 (2008).
67. Zehr, J. P. & McReynolds, L. A. Use of degenerate oligonucleotides for amplification of the *nifH* gene from the marine cyanobacterium *Trichodesmium thiebautii*. *Appl. Env. Microbiol.* **55**, 2522–2526 (1989).
68. Zehr, J. P. & Turner, P. J. Nitrogen fixation: nitrogenase genes and gene expression. *Methods Microbiol.* **30**, 271–286 (2001).
69. Parada, A. E., Needham, D. M. & Fuhrman, J. A. Every base matters: assessing small subunit rRNA primers for marine microbiomes with mock communities, time series and global field samples. *Env. Microbiol.* **18**, 1403–1414 (2016).
70. Apprill, A., McNally, S., Parsons, R. & Weber, L. Minor revision to V4 region SSU rRNA 806R gene primer greatly increases detection of SAR11 bacterioplankton. *Aquat. Microb. Ecol.* **75**, 129–137 (2015).
71. Callahan, B. J. et al. DADA2: high-resolution sample inference from Illumina amplicon data. *Nat. Methods* **13**, 581–583 (2016).
72. Moynihan, M. A. & Reeder, C. F. *nifH*dada2: v2.0.5. *Zenodo* <https://doi.org/10.5281/zenodo.7996213> (2023).
73. McLaren, M. R. & Callahan, B. J. Silva 138.1 prokaryotic SSU taxonomic training data formatted for DADA2. *Zenodo* <https://doi.org/10.5281/zenodo.4587955> (2021).
74. McMurdie, P. J. & Holmes, S. phyloseq: an R package for reproducible interactive analysis and graphics of microbiome census data. *PLoS ONE* **8**, e61217 (2013).
75. Anderson, M. J. in *Wiley StatsRef: Statistics Reference Online* (eds Kenett, R. S. et al.) (Wiley, 2017); <https://doi.org/10.1002/9781118445112.stat07841>

## Acknowledgements

This project was realized through grants from the Eurofleets+ project FIGURE, Project ANR-21-CE01-0032-01 FIESTA and Project LEFE-CYBER DEFINE2 to M.B. SPASSO (<https://spasso.mio.osupytheas.fr/>) is operated with the support of the SIP (Service Informatique de Pythéas) and in particular C. Yohia, J. Lecubin, D. Zevaco and C. Blanpain (Institut Pythéas, Marseille, France). L.I.C. was supported by Eurofleets+, LEFE/CYBER and ISblue (ANR-17-EURE-0015) project CARING. We thank the captain, crew and technicians from RV Atlantic Explorer as well as marine operations personnel at BIOS. We thank C. Le Bihan for her contributions to the biogeochemical characterization of FIGURE samples.

## Author contributions

C.H. and M.B. conceived the study. C.H. and C.C.B. processed DNA samples. C.H. performed bioinformatic and statistical analyses. O.G. ran N<sub>2</sub> fixation incubations and performed elemental analysis–isotope ratio mass spectrometry and membrane inlet mass spectrometry analyses. B.A.-G. performed the eddy statistics of the historical database archived in META3.1exp DT. B.A.-G. also identified the cyclonic eddy surveyed during the cruise in META3.0exp NRT and analysed its eddy properties. B.A.-G. searched for Argo profiles falling within and out of the cyclonic eddy of study to compute the anomaly transported by this eddy. This latter task was performed jointly with M.D.P.-H. M.D.P.-H. estimated the position of the GS from AVISO, and downloaded and analysed the available Argo profiles in the area during the time of the cruise to infer the vertical structure of the cyclonic eddy (Supplementary Fig. 2). M.D.P.-H. also downloaded and processed the surface temperature available from the Global Drifter Project and the OSTIA L4 product to create Fig. 1. S.B. set up and maintained the SPASSO package before, during and after the cruise, and analysed the SPASSO images and ADCP data during and after the cruise. A.A.P. and A.M.D. provided advice on sampling strategy and post-cruise data analysis; C.H. wrote the paper with contributions from all co-authors. All co-authors approved the current version of the paper.

## Funding

Open access funding provided by Alfred-Wegener-Institut.

## Competing interests

The authors declare no competing interests.

## Additional information

**Supplementary information** The online version contains supplementary material available at <https://doi.org/10.1038/s41561-024-01567-2>.

**Correspondence and requests for materials** should be addressed to Cora Hoerstmann, Borja Aguiar-González or Mar Benavides.

**Peer review information** *Nature Geoscience* thanks the anonymous reviewers for their contribution to the peer review of this work. Primary Handling Editor: James Super, in collaboration with the *Nature Geoscience* team.

**Reprints and permissions information** is available at [www.nature.com/reprints](http://www.nature.com/reprints).